A numerical scheme for the large-eddy simulation of turbulent combustion using a level-set method

By Laurent Duchamp de Lageneste AND Heinz Pitsch

1. Introduction

In premixed combustion, fuel and air are fully mixed before entering the combustion chamber. When a heat source is introduced (spark or pilot flame), combustion takes place in the form of a thin front propagating through the mixture. If turbulence levels are such that the reaction zone is still smaller than the Kolmogorov scale, the flame is in the flamelet regime (Peters 2000) and can be viewed as a thin interface separating two different states thus making it a suitable candidate for the use of a level-set approach.

The level-set methodology has been used in recent years to describe the dynamic evolution of fronts and discontinuities. Comprehensive overviews can be found in Sethian (1996) or Osher & Fedkiw (2002), including different possible numerical approaches and examples of applications to problems ranging from multiphase flows to image reconstruction.

The first application of this approach to the description of reacting flows is due to Williams (1985) who proposed an equation for the propagation of a flame front separating burnt from unburnt gases: the G-equation. This equation describes the evolution of a continuous field G of which a particular iso-level G_0 gives the location of the reaction front. This G_0 level is advected with the external velocity field $\mathbf{U}$, while propagating normally to itself with the laminar burning velocity s_L. The G-equation is then:

$$\frac{\partial G}{\partial t} + \mathbf{U} \cdot \nabla G = s_L |\nabla G| \,. \tag{1.1}$$

Once the position of the front is defined, one can write jump relations through the front to take gas expansion due to heat release into account, and compute all the thermochemical quantities simply from the position relative to the flame front.

Although this approach is simple and requires considerably less computational resources than solving the full system of conservation equations for the reacting species with detailed chemistry, the numerical treatment of (1.1) is generally not trivial. One difficulty arise in particular from the fact that (1.1) is strictly valid only at the particular iso-surface G_0 as can be seen by considering that the laminar burning velocity s_L can only be defined at G_0. An immediate consequence is that away from the front, the values of G are arbitrary and that the ansatz chosen should not affect the results. Theoretical considerations concerning the derivation of proper averaging procedures which respect the particular symmetries of the G-equation are discussed in Oberlack *et al.* (2001).

A common practice is to define the G field as the signed distance to the flame front (Sethian 1996). Since (1.1) will not in general conserve G as a distance as the calculation progresses, a specific procedure has to be implemented to re-assign the value of the signed distance function to points away from the front after each time step.

The numerical methods to solve the level-set equation can therefore be divided in two major steps:

- time-advance the level-set equation,
- reinitialize G to a distance function.

Because of the necessary use of upwind differencing at each stage, level-set methods have a tendency to lose surface in under-resolved regions of the flow. For applications in the RANS context (Peters 2000; Herrmann 2000) the consequences of this drawback can be expected to be small because of the relative smoothness of the mean flame front. However, the impact of these inaccuracies will grow in LES applications, where the effect of small-scale wrinkling must be retained. Attempts to improve surface conservation have led to various techniques; see Sethian (1996), Sussman & Fatemi (1999), Russo & Smereka (2000) or Peng *et al.* (1999). We will show that it is necessary to take these improvements into account if one is considering applying the level-set methodology to the LES of turbulent premixed combustion.

In this paper, we will first present the numerical methods used to advance the level-set equation in the context of LES of turbulent premixed combustion. We will then focus on some of the potential problems associated particularly with the reinitialization procedure. A detailed description of this procedure will be given, as well as some of the necessary modifications of the base algorithm that have been introduced in order to improve surface conservation properties. Finally, an example of application of the resulting method to the simulation of a laminar Bunsen flame will be presented.

2. Numerical treatment of the level-set approach for premixed combustion

In the laminar case, the G-equation flamelet model proposed by Williams (1985) yields the following equation describing the propagation of an instantaneous flame surface:

$$\frac{\partial G}{\partial t} + \mathbf{U} \cdot \nabla G = s_L |\nabla G|, \tag{2.1}$$

where $\mathbf{U}$ is the convection velocity, and s_L is the laminar burning velocity. If curvature effects are taken into account, an additional curvature correction term appears on the right-hand side of (2.1) as described by Pelce & Clavin (1982) and Matalon & Matkowsky (1982):

$$\frac{\partial G}{\partial t} + \mathbf{U} \cdot \nabla G = s_L |\nabla G| - D_M \kappa |\nabla G| \,, \tag{2.2}$$

where D_M is the Markstein diffusivity and κ the curvature.

In the LES framework, Pitsch & Duchamp de Lageneste (2002) derived the following equation for the motion of the filtered G_0 level:

$$\overline{\rho}\frac{\partial G}{\partial t} + \overline{\rho}\widetilde{\mathbf{U}} \cdot \nabla G = \frac{\rho_u}{\overline{\rho}} \left(s_T |\nabla G| - D_t \kappa |\nabla G| \right), \tag{2.3}$$

where $\widetilde{\mathbf{U}}$ is the filtered convective velocity, s_T is the modeled turbulent burning velocity and κ is the curvature of the filtered front. Here, a model for the conditionally filtered velocity derived by Pitsch in a companion article in the present volume has been introduced. In this form, (2.3) is a Hamilton-Jacobi equation with an additional parabolic curvature term.

While solutions of this equation for a given initial condition are generally not unique, Crandall & Lions (1983) showed that a unique viscosity solution can be obtained through the use of the appropriate monotone scheme. As strictly-monotone schemes are limited to first-order accuracy and are therefore too dissipative, Osher & Sethian (1988) have introduced a class of high-order upwind schemes for the Hamilton-Jacobi equation based

on the ENO polynomial reconstruction procedure previously developed by Harten *et al.* (1987) and extended by Shu & Osher (1989) in the context of conservation laws.

Here, additional difficulties can arise from local mesh refinement and the use of cylindrical coordinates. In particular, the explicit numerical treatment of the advective term would lead to unacceptably low timestep restrictions in refined regions and close to the centerline. Thus the use of an implicit scheme to treat at least parts of the advective terms is necessary.

Using mass conservation, the advective part can be rewritten in the more advantageous conservative form

$$\frac{\partial \overline{\rho} G}{\partial t} + \nabla \cdot (\overline{\rho} \mathbf{U} G) = \rho_u s_T |\nabla G| - \overline{\rho} D_t \kappa |\nabla G| \,. \tag{2.4}$$

The appropriate part of the convective terms is then treated using a semi-implicit version of the QUICK scheme described by Akselvoll (1996) and Pierce & Moin (2001) to alleviate the CFL restriction.

The propagation term appearing on the right-hand side of (2.4) is then discretized using a third-order-accurate version of the ENO scheme described by Shu & Osher (1989).

The remaining parabolic curvature term is treated accordingly, using central differences.

We will now describe the discretization of the propagation and curvature terms in more detail. The reader is referred to Akselvoll (1996) and Pierce & Moin (2001) for a thorough description of the semi-implicit scheme used to discretize the convective terms.

2.1. *Discretization of the propagation term*

Various schemes have been derived for the numerical treatment of the propagation term appearing in (2.4). The two most popular variants are the Engquist-Osher entropy-satisfying scheme and the Godunov scheme.

Our objective is to discretize the term $s_T \cdot |\nabla G|$ appearing in (2.4), rewritten in the following form:

$$s_T \cdot |\nabla G| = \max(s_T, 0)\nabla^+ + \min(s_T, 0)\nabla^-. \tag{2.5}$$

The Engquist-Osher scheme to obtain ∇^+ and ∇^- would then read

$$\begin{aligned} \nabla^+ = \Big[& max(D_{-x}^{i,j,k}, 0)^2 + min(D_{+x}^{i,j,k}, 0)^2 \\ & + max(D_{-y}^{i,j,k}, 0)^2 + min(D_{+y}^{i,j,k}, 0)^2 \\ & + \; max(D_{-z}^{i,j,k}, 0)^2 + min(D_{+z}^{i,j,k}, 0)^2 \Big]^{1/2} \,, \end{aligned} \tag{2.6}$$

and

$$\begin{aligned} \nabla^- = \Big[& max(D_{+x}^{i,j,k}, 0)^2 + min(D_{-x}^{i,j,k}, 0)^2 \\ & + max(D_{+y}^{i,j,k}, 0)^2 + min(D_{-y}^{i,j,k}, 0)^2 \\ & + \; max(D_{+z}^{i,j,k}, 0)^2 + min(D_{-z}^{i,j,k}, 0)^2 \Big]^{1/2} \,, \end{aligned} \tag{2.7}$$

while the Godunov scheme is given by:

$$\begin{aligned} \nabla^+ = \Big[& max(max(D_{-x}^{i,j,k}, 0)^2, min(D_{+x}^{i,j,k}, 0)^2) \\ & + max(max(D_{-y}^{i,j,k}, 0)^2, min(D_{+y}^{i,j,k}, 0)^2) \end{aligned} \tag{2.8}$$

$$+ \; max(max(D^{i,j,k}_{-z},0)^2, min(D^{i,j,k}_{+z},0)^2)\Big]^{1/2} \;,$$

and

$$\begin{aligned}\nabla^- = \Big[&max(max(D^{i,j,k}_{+x},0)^2, min(D^{i,j,k}_{-x},0)^2)\\ &+ max(max(D^{i,j,k}_{+y},0)^2, min(D^{i,j,k}_{-y},0)^2)\\ &+ \; max(max(D^{i,j,k}_{+z},0)^2, min(D^{i,j,k}_{-z},0)^2)\Big]^{1/2} \;,\end{aligned} \tag{2.9}$$

where $D^{i,j,k}_{\pm x,\pm y,\pm z}$ are third-order ENO approximations to the gradient of G in each direction.

Although both methods should give equivalent results, the Godunov scheme is generally considered to be slightly less dissipative near sonic points than the Engquist-Osher scheme, and will be used to discretize the propagation term.

2.2. *Discretization of the curvature term*

The curvature term, being parabolic in nature, is accordingly discretized using second-order central differencing (Sethian 1996).

Introducing the mean curvature as

$$\kappa_M = \nabla \cdot \mathbf{N_G} = -\nabla \cdot \frac{\nabla \mathbf{G}}{|\nabla G|} \,, \tag{2.10}$$

where $\mathbf{N}_G = -\nabla G/|\nabla G|$ is the normal to each iso-level of G, the term $D_t\kappa|\nabla G|$ in (2.3) is discretized as

$$D_t\kappa|\nabla G| = D_t\kappa^{i,j,k}_M \left[(D^{i,j,k}_{cx})^2 + (D^{i,j,k}_{cy})^2 + (D^{i,j,k}_{cz})^2\right]^{1/2} \;, \tag{2.11}$$

where $\kappa^{i,j,k}_M$ is a central-difference approximation of the expression given in (2.10 and $D^{i,j,k}_{cx,cy,cz}$ is the second-order central-difference approximation of the components of the gradient of G in each direction.

3. Reinitialization

In problems such as turbulent combustion, it is impossible to maintain the level-set function as a signed distance from the moving G_0 surface because of the turbulent nature of the advective flow field. Flat or steep regions develop as the interface moves, rendering computation at these places inaccurate. It is therefore necessary to introduce a procedure that will reset the G-field to the signed distance from G_0 in a pre-defined neighborhood of G_0. Such a procedure is called reinitialization and several variants have been proposed by Sethian (1996), Sussman & Fatemi (1999), Russo & Smereka (2000) and Peng *et al.* (1999).

In LES, where the effects of small-scale motion on the front must be retained, special attention must be paid to using a procedure that preserves the position of the G_0-surface accurately.

3.1. *General procedure*

In order to reset the G field to the signed distance from the G_0 surface, the following equation has to be solved to a steady state:

$$\phi_0 = G(x,0) \tag{3.1}$$

$$\frac{\partial \phi}{\partial t} = S(\phi_0)(1 - |\nabla \phi|)\,, \tag{3.2}$$

where $S(\phi_0)$ is a smoothed sign function defined by

$$S(q) = \frac{q}{\sqrt{q^2 + \Delta x^2}}\,. \tag{3.3}$$

It is possible to rewrite (3.2) as an advection equation,

$$\frac{\partial \phi}{\partial t} + \mathbf{w} \cdot \nabla \phi = S(\phi_0) \tag{3.4}$$

$$\mathbf{w} = S(\phi_0)\frac{\nabla \phi}{|\nabla \phi|}\,. \tag{3.5}$$

A suitable numerical scheme can then be derived from those developed for solving the advection equation.

We use a third-order ENO scheme presented in Shu & Osher (1989) or Sussman & Fatemi (1999) for the spatial derivatives, while time advancement is done using the corresponding third-order optimal Runge-Kutta scheme.

One then obtains the following Godunov scheme for the reinitialization (expressed for a first-order time discretization, for simplicity):

$$\phi_0 = G(x, 0) \tag{3.6}$$

$$\phi^{n+1} = \phi^n + dt\left[max(S(\phi_0), 0)\nabla^+ + min(S(\phi_0), 0)\nabla^-\right]\,, \tag{3.7}$$

with

$$\begin{aligned}\nabla^+ = 1 - \Big[&max(max(D^{i,j,k}_{-x}, 0)^2, min(D^{i,j,k}_{+x}, 0)^2) \\ &+ max(max(D^{i,j,k}_{-y}, 0)^2, min(D^{i,j,k}_{+y}, 0)^2) \\ &+ max(max(D^{i,j,k}_{-z}, 0)^2, min(D^{i,j,k}_{+z}, 0)^2)\Big]^{1/2}\,,\end{aligned} \tag{3.8}$$

and

$$\begin{aligned}\nabla^- = 1 - \Big[&max(max(D^{i,j,k}_{+x}, 0)^2, min(D^{i,j,k}_{-x}, 0)^2) \\ &+ max(max(D^{i,j,k}_{+y}, 0)^2, min(D^{i,j,k}_{-y}, 0)^2) \\ &+ max(max(D^{i,j,k}_{+z}, 0)^2, min(D^{i,j,k}_{-z}, 0)^2)\Big]^{1/2}\,,\end{aligned} \tag{3.9}$$

where $D^{i,j,k}_{\pm x,\pm y,\pm z}$ are third-order ENO approximations of the components of the gradient of ϕ in each direction.

Once a stationary solution is obtained for ϕ, G is simply replaced by ϕ.

3.2. *Reinitialization in presence of high or low gradients*

3.2.1. *General procedure*

When advected by a turbulent velocity field, regions of high or low gradient are likely to develop around the G_0-surface. When the procedure outlined above is applied, Peng *et al.* (1999) have shown that large straying of the G_0 surface may occur, especially in high gradient regions, while convergence in regions of low gradients tends to be slow.

Peng *et al.* (1999) proposed a modification of this method, designed to avoid these drawbacks by taking the local value of the gradient into account in smoothing of the sign function.

In this variant, the sign function is now given by:

$$S(q) = \frac{q}{\sqrt{q^2 + |\nabla G|^2 \Delta x^2}} \,. \tag{3.10}$$

As noted by Osher & Fedkiw (2002), for this procedure to work well it is necessary to update $S(q)$ continuously as the calculation progresses.

An illustration of the improvements achieved using this formulation is given in the next section.

3.2.2. *Validation: one time reinitialization of a distorted field*

To assess the ability of this method to conserve the initial location of the G_0 level if regions of high or low gradient are present, we compare the results of the reinitialization of the ϕ_0 field (Russo & Smereka 2000),

$$\phi_0 = f(x,y) \left[\sqrt{\frac{x^2}{A^2} + \frac{y^2}{B^2}} - 1 \right] , \tag{3.11}$$

to a signed distance function.

Here, $f(x,y) = \epsilon + (x - x_0)^2 + (y - y_0)^2$, with $A = 4$, $B = 2$, $\epsilon = 0.1$, $x_0 = 3.5$, and $y_0 = 2$. Hence, the $\phi_0 = 0$ surface is an ellipse and is surrounded by both high and low gradients (see figure 1).

The computational domain is $\Omega = [-5, 5] \times [-5, 5]$ and a coarse, 50×50, grid is used.

Results of the reinitialization using the sign function defined in (3.3) are presented in figure 1. Reinitialization across the $\phi_0 = 0$ surface results in undesired perturbations that can be considerable in regions of larger gradients.

In figure 2, results using the sign function defined by (3.10 show that straying of the $\phi_0 = 0$ surface is avoided in the high-gradient zone.

Another positive side-effect of this modification can be observed in low-gradient regions where the modification of the sign function leads to faster convergence of the procedure. This is particularly apparent in the comparison of the results obtained in the upper-right corner region after ten iterations with both methods.

3.3. *Enforcing volume conservation*

The procedure outlined above is a third-order space- and time-accurate method to achieve reinitialization of the G-field. However, as pointed out by Sussman & Fatemi (1999), because of its upwind nature, its direct application may lead to unwanted dissipation of the G_0-surface. Furthermore, the reinitialization error is likely to accumulate as the number of time steps grows.

This effect can be expected to be even more pronounced when G exhibits regions of locally-large curvature like small wrinkles of the flame surface.

Sussman & Fatemi (1999) proposed a constraint that prevents straying of the G_0 surface, and has the additional advantage that the error introduced is independent of the number of time steps required to reinitialize the G-field.

Noting that the volume enclosed in the G_0 surface can be evaluated by

$$V = \int S(G) d\mathbf{x} \,, \tag{3.12}$$

where $S(G)$ is the smoothed approximation of the sign function appearing in (3.2), volume

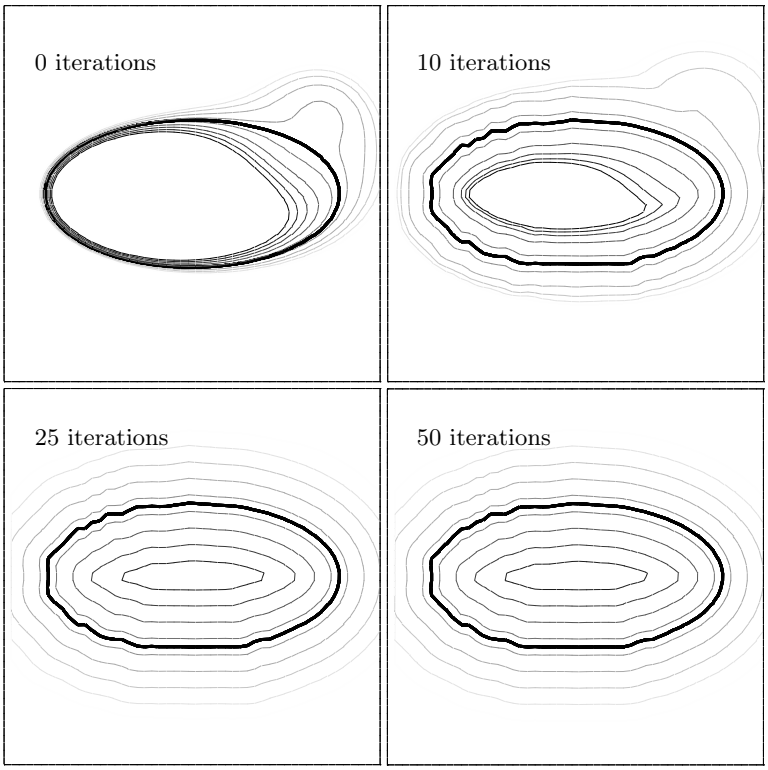

FIGURE 1. One time reinitialization with sign function defined by (3.3) on a 50×50 grid. From left to right and top to bottom, reinitialized field after 0, 10, 25 and 50 iterations. The $G_0 = 0$ level is displayed as a bold line.

conservation is enforced by requiring that

$$\partial_t \int S(G) d\mathbf{x} = 0\,. \tag{3.13}$$

By introducing the operator $L(\phi_0, \phi) = S(\phi_0)(1 - |\nabla\phi|)$, the reinitialization procedure becomes

$$\frac{\partial \phi}{\partial t} = L(\phi_0, \phi) + \lambda f(\phi)\,, \tag{3.14}$$

where λ is obtained by requiring that

$$\partial_t \int S(G) = \int S'(\phi)\frac{\partial \phi}{\partial t} = \int S'(\phi)(L(\phi_0, \phi) + \lambda f(\phi)) = 0\,. \tag{3.15}$$

Taking $f(\phi) = S'(\phi)|\nabla\phi|$ leads to

$$\lambda = \frac{-\int S'(\phi) L(\phi_0, \phi)}{\int S'(\phi)^2 |\nabla\phi|}\,, \tag{3.16}$$

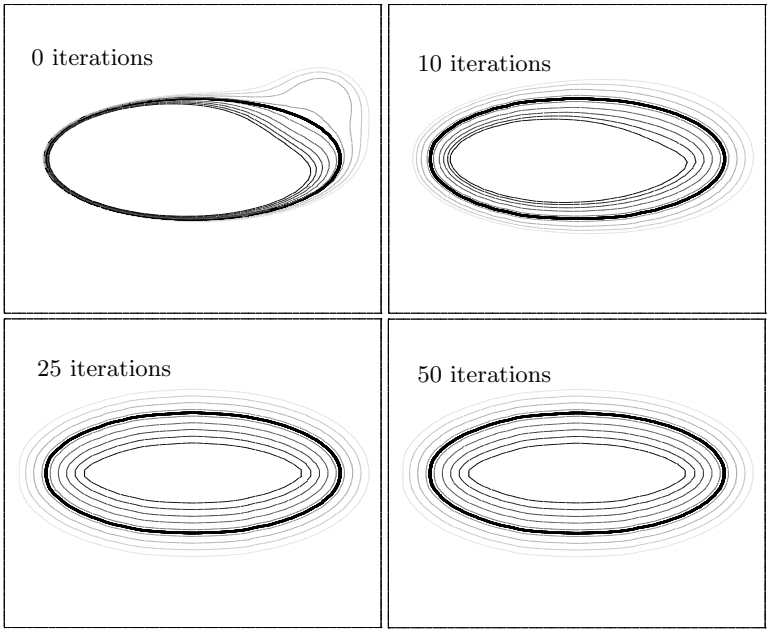

FIGURE 2. One time reinitialization with sign function defined by (3.10) on a 50×50 grid. From left to right and top to bottom, reinitialized field after 0, 10, 25 and 50 iterations. The $G_0 = 0$ level is displayed as a bold line.

with

$$S'(q) = \frac{\Delta x^2}{[q^2 + \Delta x^2]^{\frac{3}{2}}}\,. \tag{3.17}$$

This leads to the new procedure:

(*a*) Solve $\widetilde{\phi}_{n+1} = \phi_n + dtL(\phi_0, \phi)$ using the same third-order ENO scheme described in section 3.1.

(*b*) Solve $\phi_{n+1} = \widetilde{\phi}_{n+1} + dt\lambda S'(\phi_0)|\nabla\phi_0|$ to get the constrained solution of the reinitialization sub-step where the terms $S'(\phi)$, $L(\phi_0, \phi)$ and $f(\phi)$ appearing in (3.14) and (3.16) are discretized as $S'(\phi_0)$, $\frac{\widetilde{\phi}_{n+1} - \phi_0}{dt}$, and $S'(\phi_0)|\nabla\phi_0|$ respectively.

When a Runge-Kutta fractional step method is used for the time discretization, the constraint is enforced only once at the end of each time step. All the integrals are evaluated using a third-order Simpson's rule on a nine-point stencil.

An illustration of the improvements obtained using this constraint is provided in the next section.

3.3.1. *Zalesak's problem*

Zalesak's problem involves the rotation of a notched circle and constitutes a good test of how well the reinitialization handles regions of high curvature.

The domain is a square of 100×100, where a notched circle is centered at $(25, 0)$. The

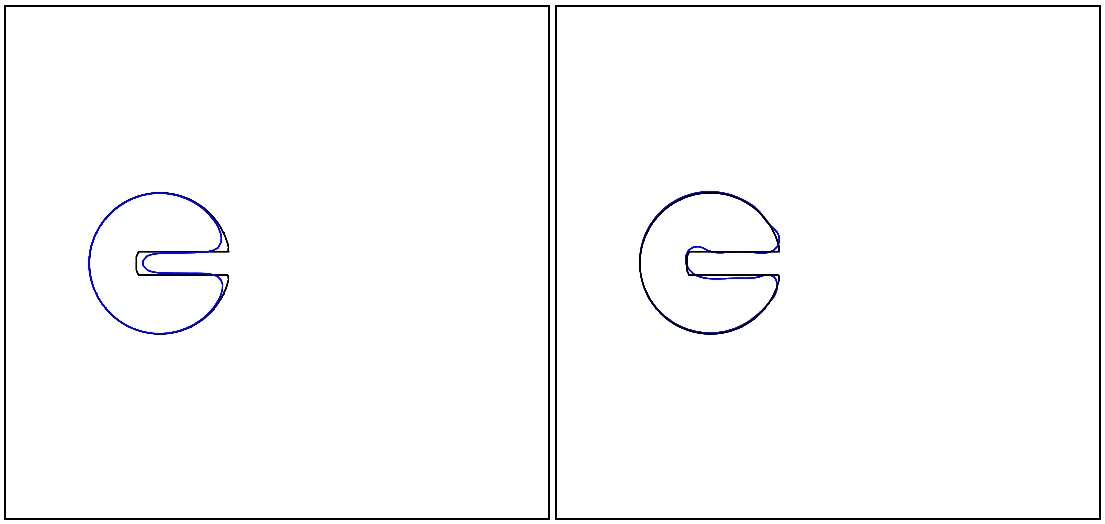

FIGURE 3. Zalesak's problem after one full revolution on a 100×100 grid, reinitialization alone (left) and reinitialization with volume-preservation constraint (right).

velocity field is constant in time and is defined as

$$U = \frac{(50 - y)\pi}{314},$$
$$V = \frac{(x - 50)\pi}{314}.$$

The results after one full revolution around the center of rotation are shown in figure 3. On the left side is the result obtained using reinitialization without the constraint, and on the right is the result of the computation using the constraint. Both results are compared to the analytical solution. While results of both methods are very good for the circular region of the object, important differences are found in the rectangular region where the method without constraint is shown to round off the sharp corners, leading to a surface loss of nearly 10%.

Using the constraint, sharp corners are better preserved and surface loss is only about 2%.

4. Validation: numerical simulation of a laminar Bunsen flame (Echekki & Mungal 1990)

As a first validation of the numerical scheme we use in the case of reacting flows, we present results obtained from the numerical simulation of a laminar Bunsen flame in this section.

This configuration has been studied experimentally by Echekki & Mungal (1990) and consists of a rectangular 2-D slot burner with an exit section width of $H = 6.8\,\mathrm{mm}$. The exit velocity is $U_0 = 1.5\,\mathrm{m/s}$ and the fuel is a stoichiometric mixture of methane and air.

The 2-D numerical simulation domain is $6H$ long and $6H$ wide. The inlet profile is set to be a top-hat profile and a boundary layer is allowed to develop for $1H$ before the flow exits the burner.

Figure 4 shows a comparison of the position of the flame front observed in the experiment with the results of the simulation, together with a visualization of the streamlines.

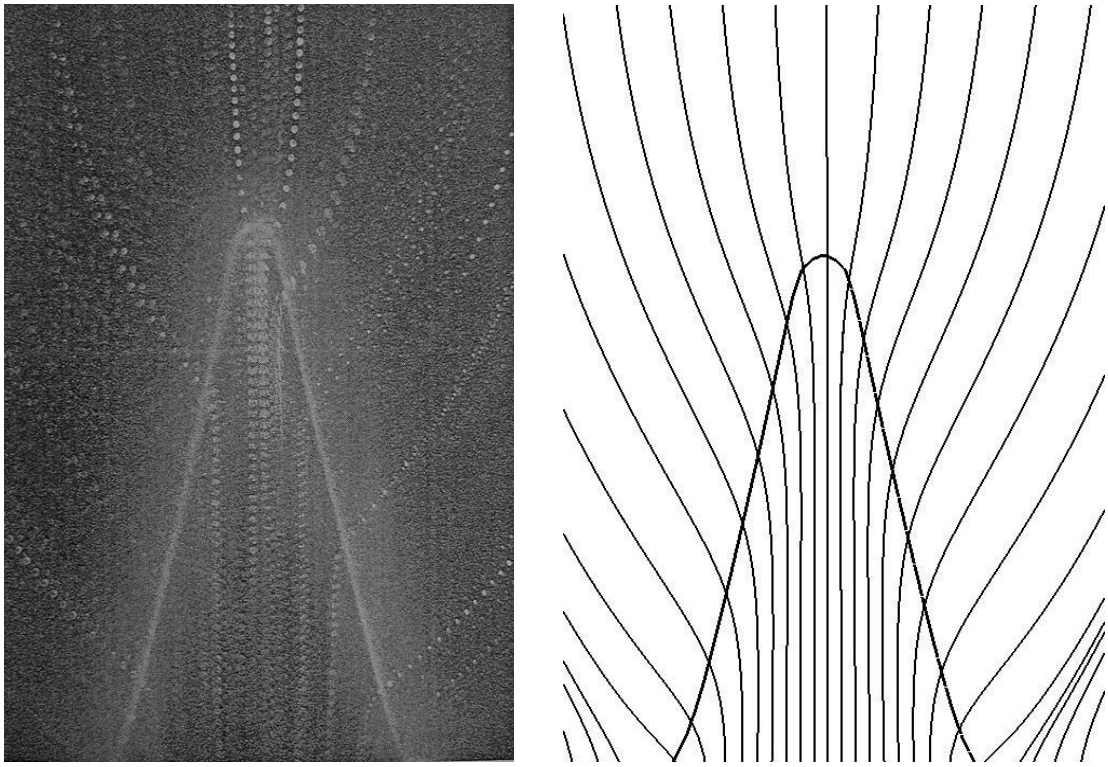

FIGURE 4. Laminar Bunsen flame: flame position and streamlines. Experiment (left) and simulation (right).

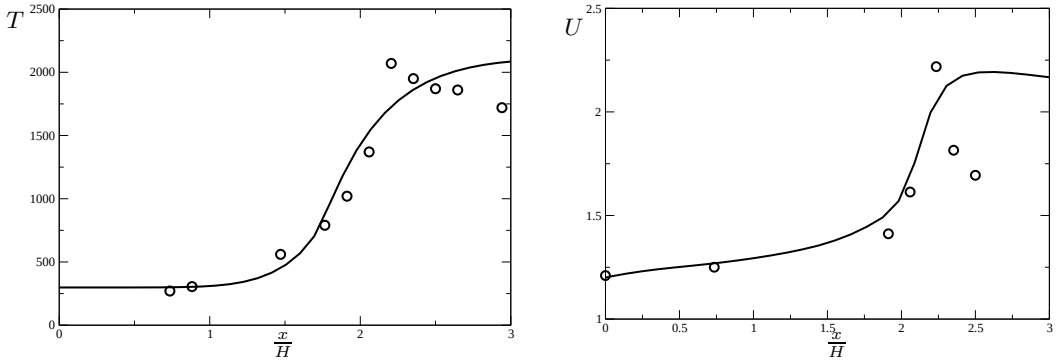

FIGURE 5. Laminar Bunsen flame: Temperature (left) and velocity (right). Experimental results (symbols) and numerical simulation (solid lines).

Good agreement is obtained for the flame length as well as for the curvature at the tip of the flame, showing that the increase in flame speed due to curvature is well reproduced by the simulation. A similar divergence of the streamlines in the burned region of the flame can be observed, showing that the simulation also predicts the effect of heat release on the flow field correctly.

Figure 5 shows the evolution of temperature (left) and axial velocity (right) along

the axis of symmetry of the flame. The temperature rise along the axis as well as the simultaneous velocity increase are well predicted by the simulation until the tip is reached. Behind the flame tip however, the temperature in the experimental data drops slowly due to radiation, which is neglected in our simulation. The simulation therefore predicts nearly-constant temperature behind the tip.

As a consequence, the fast deceleration of the gas downstream of the tip is also underestimated in the simulation.

5. Conclusion

In this report, we have presented numerical methods to solve the level-set equation for premixed combustion in LES. In particular, we have described the third-order ENO scheme used to discretize the normal propagation term as well as the numerical schemes used for the remaining terms.

We have then stressed that the reinitialization procedure used to keep G as a distance function is a key factor in the development of an accurate level-set model for LES of turbulent premixed combustion. The overall method, including its discretization by an higher-order ENO scheme has been introduced. Examples of potential problems generated by the application of this algorithm to the case of turbulent combustion have been given. Consequently, a first modification of the procedure has been introduced to avoid undesired straying of the interface due to the creation of regions of low or high gradients due to the turbulence. An additional constraint has been implemented in order to enforce volume conservation around the flame surface.

A first validation of the resulting scheme has finally been presented for the case of a laminar Bunsen flame, showing reasonable agreement with experimental data.

Further applications of this method in LES of turbulent premixed flames are reported in a companion paper in this volume.

Acknowledgments

The authors gratefully acknowledge funding by the US Department of Energy within the ASCI program and by SNECMA Moteurs.

REFERENCES

Akselvoll, K. 1996 An efficient method for temporal integration of the navier-stokes equations in confined axisymmetric geometrie. *J. Comp. Phys.* **125**, 454–463.

Crandall, M. G. & Lions, P. L. 1983 Viscosity solutions of Hamilton-Jacobi equations. *Trans. Amer. Math. Soc.* **277**, 1–42.

Echekki, T. & Mungal, M. G. 1990 Flame speed measurements at the tip of a slot burner: effects of flame curvature and hydrodynamic stretch. In 23^{rd} *Symposium on Combustion* (ed. T. C. Institute), pp. 455–461.

Harten, A., Engquist, B., Osher, S. & Chakravarthy, S. 1987 Uniformly high order accurate essentially non-oscillatory schemes III. *J. Comp. Phys.* **71**, 231–303.

Herrmann, M. 2000 Numerische simulation vorgemischter und teilweise vorgemischter turbulenten flamen. PhD thesis, RWTH, Aachen.

Matalon, M. & Matkowsky, B. J. 1982 Flames as gasdynamic discontinuities. *J. Fluid Mech.* **124**, 239–259.

Oberlack, M., Wenzel, H. & peters, N. 2001 On symmetries and averaging of the G-equation for premixed combustion. *Comb. Theo. and Model.* **5**, 1–20.

Osher, S. & Fedkiw, R. 2002 *Level set methods and dynamic implicit surfaces*, *Applied Mathematical Sciences*, vol. 153. Springer, Berlin.

Osher, S. & Sethian, J. 1988 Fronts propagating with curvature dependant speed: algorithms based on Hamilton-Jacobi formulations. *J. Comp. Phys.* **79**, 12–49.

Pelce, P. & Clavin, P. 1982 Influence of hydrodynamic and diffusion upon the stability limits of laminar premixed flames. *J. Fluid Mech.* **124**, 219–237.

Peng, D., Merriman, B., Osher, S., Zhao, H. & Kang, M. 1999 A PDE-based fast local level set method. *J. Comp. Phys.* **155**, 410–438.

Peters, N. 2000 *Turbulent Combustion*. Cambridge University Pres.

Pierce, C. D. & Moin, P. 2001 Progress-variable approach for large eddy simulation of turbulent combustion. *Tech. Rep.* TF-80. Dept. Mech. Eng., Stanford University.

Pitsch, H. & Duchamp de Lageneste, L. 2002 Large-eddy simulation of premixed turbulent combustion using a level-set approach. In *Proceedings of the 29th Symposium on Combustion*. The Combustion Institute: accepted for publication.

Russo, G. & Smereka, P. 2000 A remark on computing distance functions. *J. Comp. Phys.* **163**, 51–67.

Sethian, J. A. 1996 *Level Set Methods : Evolving Interfaces in Geometry, Fluid Mechanics, Computer Vision and Material Science*. Cambridge University Press.

Shu, C. W. & Osher, S. 1989 Efficient implementation of essentially non-oscillatory shock capturing schemes, II. *J. Comp. Phys.* **83**, 32–78.

Sussman, M. & Fatemi, E. 1999 An efficient, interface-preserving level set re-distancing algorithm and its application to interfacial incompressible fluid flow. *SIAM Journ. Sci. Comp.* **20**, 1165–1191.

Williams, F. A. 1985 Turbulent combustion. In *The Mathematics of Combustion* (Frontiers in Applied Mathematics, vol. 2, J. Buckmaster, ed.) SIAM, Philadelphia, pp. 97–131.